Hindawi
Geofluids
Volume 2022, Article ID 2352386, 13 pages
https://doi.org/10.1155/2022/2352386

Research Article

Effects of Cavities on Lining Structure behind Cold Zone Tunnels Based on Coupled Thermal Analysis

Xian Xiao [1,2] **and Jianwei Nie** [3]

[1]*School of Civil Engineering, Southeast University, Nanjing 210000, China*
[2]*Guiyang City-Invest Green Industrial Co., Ltd., Guiyang 550000, China*
[3]*PowerChina Kunming Engineering Corporation Limited, Kunming 650000, China*

Correspondence should be addressed to Xian Xiao; 230209075@seu.edu.cn

Received 20 March 2022; Revised 26 April 2022; Accepted 24 August 2022; Published 13 September 2022

Academic Editor: S. P. Pradhan

Copyright © 2022 Xian Xiao and Jianwei Nie. This is an open access article distributed under the Creative Commons Attribution License, which permits unrestricted use, distribution, and reproduction in any medium, provided the original work is properly cited.

There is a significant difference between ambient temperature and internal temperature of surrounding rock in the cold season. Based on the Dulongjiang (DLJ) Tunnel, this paper studies the influence of frost heave force on lining structure and establishes a thermos-dynamical coupling model using the field. The results show that the environmental temperature and the cavity behind the lining greatly influence the safety of the tunnel structure. The internal force of the tunnel lining increases with the decrease of the environmental temperature and stress. The existence of a water-bearing cavity causes the deformation of the vault position to improve and advance. In contrast, the deformation presence of a water-bearing hole causes the deformation of the vault position to increase and reach, while the deformation time of the arch foot position to delay.

1. Introduction

One of the critical issues is the effect of freezing and thawing. In China's cold region tunnels, seasonal cold region tunnels are subject to severe climatic conditions during the cold season, especially for existing tunnels that have suffered structural damage due to improper construction and operational maintenance. In Russia and some tunnels in the northeast and northwest China, hanging ice in tunnels, ice on roadways, and water leaks in tunnels have been observed [1–5]. The problem is that the tunnel lining has been damaged. It is inaccurate to explain the causes of freezing damage in cold tunnels by saying that the tunnel lining is cracked and damaged by the freezing and swelling of the surrounding rock. In such cold tunnels, the leading cause of frost damage is the pressure of the lining caused by the freezing and swelling of the water that accumulates behind the lining. The irregularity of the excavation surface in cold zone tunnels often results in the construction process not being a tight fit between the surrounding rock and the lining structure but instead leaving behind-wall voids between the lining and the surrounding rock. Most of this space exists in the vault area and is mainly caused by the concrete pouring process and the concrete's cumulative deformation during hydration [6–10].

Therefore, to solve the problem of frost damage in existing damaged tunnels located in cold areas, it is necessary to conduct a study on the coupling analysis of temperature and stress fields in cold area tunnels. Scholars at home and abroad have shown a wealth of research on this subject [11–16]. Lai et al. [17–19] carried out a coupled nonlinear analysis of temperature, seepage, and stress fields in cold tunnels. Theoretical derivations and numerical calculations were carried out for the nonlinear temperature field of the cold region tunnel using the Galerkin method (Zhang et al. [20, 21]). Xie et al. [22] used the finite element calculations combined with field tests to study the effect of insulation on the lining for the phase change problem. Yuan et al. [23] proposed a numerical solution to the phase change heat conduction problem utilizing the finite difference method. Theoretical analysis and simplified calculation based on engineering for the distribution of freezing and expansion

forces in cold zone tunnels have achieved good results (Xia et al. [24]). However, water-bearing cavities behind the lining inevitably complicate the structural forces and shapes on the structural safety of mountain tunnel liners. Yuan et al. [25] established a load calculation model for the problem of cavities behind the lining through theoretical analysis. Wang and Zheng [26] established two simplified models for frost heave of water behind the liner and quantified the internal force influence law and error of frost heave force behind the liner. Li and Chen [27] introduced a method to solve the frost heave force and frost heave deformation considering water behind the liner using the theory of complex functions: Gao et al. [28] used indoor model tests to investigate the effect of frost heave on different locations and volumes of water behind the tunnel liner.

Comprehensive analysis shows that scholars are currently inclined to study the impact of different cavity forms on the structure and to determine the suitable thickness of the insulation layer in order to achieve the insulation effect and reduce the cost at the same time; few scholars have compared and studied the magnitude of the impact of insulation and water-bearing cavities on the structure. In a comprehensive analysis, scholars mainly study the temperature field in the tunnel and the stress field and the nonlinear coupling of the seepage field according to determine the appropriate insulation measures; for the lining behind the cavity problem, the academic system is biased toward the study of the cavity form on the safety of the lining structure, and for the temperature, effect combined with the cavity to consider the law of its impact on the lining less research.

This paper relies on the Dulongjiang Tunnel to establish a thermodynamic coupling analysis model considering the temperature effect and cavity structure. The paper studies the influence of ambient temperature and water-bearing cavity behind the lining on the internal force and displacement of the lining structure, and the results of which can provide suggestions for the operation and maintenance of this project and provide a reference for similar projects.

2. Project Background

The Dulongjiang Tunnel is located on the Dulong River Highway, about 40 km from Gongshan County. The tunnel was completed and opened to traffic in 2014. The tunnel starts at mileage K158+802 to K165+482, with a total length of 6,680 m, a single cavern two-lane tunnel running in opposite directions. The tunnel is designed to have a net width of 8.5 m, a net height of 6.8 m, an end-wall door, cross ventilation, drainage for the roadside of the cave, and a concrete road surface. The tunnel suffers from poor drainage at the top of the cavern, cracking of the lining, and cavities behind the lining. The tunnel is also located in an alpine area, and avalanches have damaged the power supply lines during operation. The DLJ tunnel location is shown as Figure 1.

3. Heat Transfer Theory Analysis for Tunnels in Cold Regions

3.1. Basic Assumptions. The tunnel is a complex structural body, and to obtain theoretical solutions for the tunnel lining and envelope temperature fields, the following simplifications and assumptions are made.

(1) The actual tunnel section is in the form of a horseshoe, very close to a circle, and for calculating, the actual section is considered as a circular section

(2) The thermal resistance of the contact between the insulation and the second lining, the second lining and the primary lining, and the lining and the surrounding rock is not considered, and the persistent condition of equal temperature and heat flow is satisfied at the contact boundary

(3) The tunnel lining and surrounding rock are normothermic, i.e., the thermal conductivity, specific heat capacity, and density do not change with temperature

(4) Considering only the heat transfer occurring in the radial direction in the tunnel envelope, the heat transfer in the tunnel envelope is calculated as two-dimensional heat transfer

(5) Equal air temperature at any location within the tunnel cross-section

(6) Unfrozen soil in the cavity behind the wall is considered to be isotropic material

(7) Disregarding heat migration during water transfer from the liquid to the solid-state

(8) The pressure value at which water changes to ice remains the same

3.2. Radial Heat Transfer in the Tunnel. Tunnel excavation will affect the original temperature field of the surrounding rock within a specific area (the tunnel temperature field influences circle). The temperature of the surrounding rock within the influence circle is affected by both the temperature inside the cave and the surface temperature. In contrast, the temperature field of the surrounding rock outside the influence circle is only affected by the surface temperature and is not affected by the tunnel excavation. For the convenience of theoretical calculations, the influence radius r_d of the temperature field of the tunnel surrounding rock is used to describe the influence circle of the tunnel temperature field quantitatively, and the thickness of the influence circle of the tunnel temperature field is $6 \sim 10$ m under general conditions.

A sketch of the temperature field calculation in a cold tunnel is shown in Figure 2. In Figure 2: r and θ are the parameters of the polar coordinate system. The heat transfer of the tunnel surrounding rock considering the lining and insulation is a circular multilayer medium heat transfer problem. The circular multilayer medium heat transfer

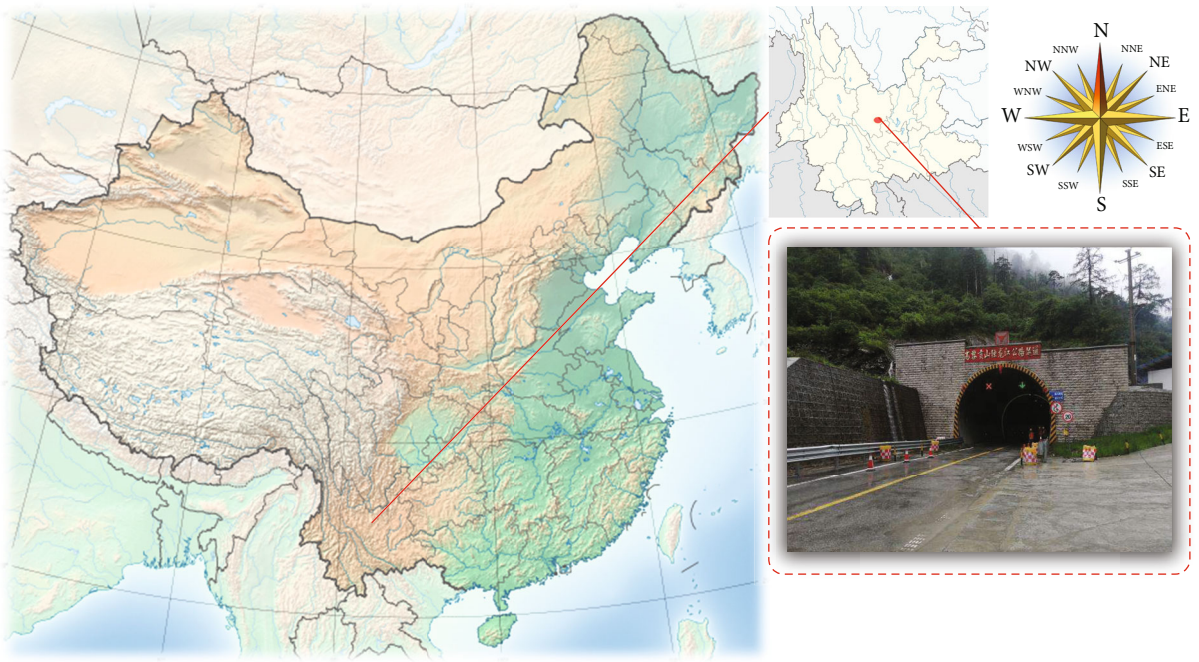

Figure 1: The DLJ tunnel location.

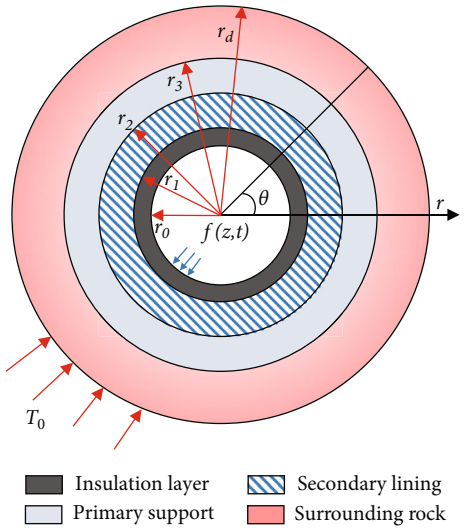

Figure 2: Temperature field calculation sketch of tunnel.

theory establishes the tunnel heat transfer equation considering the lining and insulation. The heat transfer equations for insulation, second lining, primary lining, and perimeter rock are as follows

$$\frac{\partial^2 T_1}{\partial r^2}(r,t)+\frac{1}{r}\frac{\partial T_1}{\partial r}(r,t)=\frac{1}{\alpha_1}\frac{\partial T_1}{\partial t}(r,t), \tag{1}$$

$$\frac{\partial^2 T_2}{\partial r^2}(r,t)+\frac{1}{r}\frac{\partial T_2}{\partial r}(r,t)=\frac{1}{\alpha_2}\frac{\partial T_2}{\partial t}(r,t), \tag{2}$$

$$\frac{\partial^2 T_3}{\partial r^2}(r,t)+\frac{1}{r}\frac{\partial T_3}{\partial r}(r,t)=\frac{1}{\alpha_3}\frac{\partial T_3}{\partial t}(r,t), \tag{3}$$

$$\frac{\partial^2 T_4}{\partial r^2}(r,t)+\frac{1}{r}\frac{\partial T_4}{\partial r}(r,t)=\frac{1}{\alpha_4}\frac{\partial T_4}{\partial t}(r,t), \tag{4}$$

where $T_1 \sim T_4$ are the insulation temperatures, secondary lining, initial lining, and surrounding rock, respectively; $\alpha_1 \sim \alpha_4$ are the thermal diffusion coefficients of insulation, secondary lining, initial support, and surrounding rock, respectively; t is time.

The forced convective heat exist in the cave air and the cave wall.

$$-k_1\frac{\partial T_1}{\partial r}(r_0,t)=-h(T_1(r_0,t)-f(z,t)). \tag{5}$$

$f(z,t)$ is the air temperature field inside the tunnel.

The shallow depth of the tunnel is subject to both surface air temperature and in-cavity air temperature, resulting in very complex temperature distribution and a phase change in the surrounding rock outside the circle of influence in winter. From Figure 2, in order to obtain the temperature field of a shallow buried tunnel, the temperature at the outer boundary of the influence circle needs to be determined. So that the temperature field of the tunnel lining and the surrounding rock can be calculated based on the temperature inside the cavern and the temperature at the outer boundary of the influence circle.

When the surface air temperature is below the phase change temperature of the water, the temperature field of the rock below the surface consists of 3 zones: the frozen zone, the mixed zone, and the unfrozen zone (Figure 3).

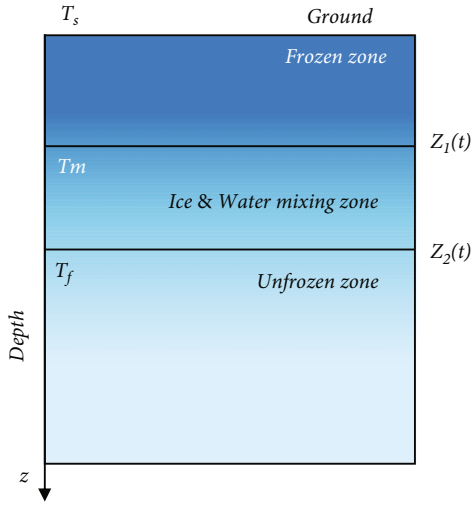

Figure 3: Calculation model of surrounding rock temperature field under surface.

The temperature field distribution in the frozen, mixed, and unfrozen zones is calculated as follows:

$$T_{1d}(z,t) = (T_m - T_s)\cdot \frac{T_1\left(z\sqrt{\alpha_1 t/2}\right)}{f_1(\psi)} + T_s \quad 0 \le z \le Z_1(t), \tag{6}$$

$$T_{2d}(z,t) = \left(T_m - T_f\right)\frac{f_1(z\sqrt{\alpha_4 t}/2) - f_1(\gamma)}{f_1(\gamma) - f_1\left(\psi\sqrt{\alpha_1/\alpha_4}\right)} + T_f \quad Z_1(t) < z \le Z_2(t), \tag{7}$$

$$T_{3d}(z,t) = \left(T_f - T_0\right)\frac{f_2(z\sqrt{\alpha_3 t}/2)}{f_2(\gamma\sqrt{\alpha_4/\alpha_3})} + T_0 \quad z \ge Z_2(t), \tag{8}$$

where $T_{1d}(z,t)$, $T_{2d}(z,t)$, and $T_{3d}(z,t)$ are the temperatures in the frozen, mixed, and unfrozen zones, respectively; $Z_1(t)$ is the ice and water mixing moving boundary, $Z_1(t) = 2\psi\sqrt{\alpha_1 t}$; $Z_2(t)$ is the frozen surface, $Z_2(t) = 2\gamma\sqrt{\alpha_4 t}$; T_s is the minimum monthly mean surface temperature; T_m is the temperature at which water is completely converted to ice; T_f is the temperature at which the phase change occurs; z is the depth of the soil layer; $f_1(\bullet)$ is the error function; $f_2(\bullet)$ is the complementary error function. The following equations determine the parameters ψ and γ.

$$\frac{T_m - T_s}{T_m - T_f}e^{-\psi^2(1-a_1/a_4)} = \frac{k_2}{k_1}\sqrt{\frac{\alpha_1}{\alpha_4}}\cdot\frac{f_1(\psi)}{f_1(\gamma) - f_1\left(\psi\sqrt{\alpha_1/\alpha_4}\right)}, \tag{9}$$

$$\frac{T_m - T_f}{T_0 - T_2}\frac{\alpha_2}{k_3}\sqrt{\frac{\alpha_3}{\alpha_4}}e^{-\gamma^2(1-\alpha_1/a_4)} = \frac{f_1(\gamma) - f_1\left(\psi\sqrt{\alpha_1/\alpha_4}\right)}{f_2(\gamma\sqrt{\alpha_4/a_3})}, \tag{10}$$

$$\begin{aligned} a_1 &= \frac{k_1}{c_1}, \\ \alpha_3 &= \frac{k_3}{c_3}, \end{aligned} \tag{11}$$

$$\alpha_4 = \frac{k_2}{c_2 + (1-\varepsilon)\rho_r L_i \Delta\xi/\left(T_f - T_m\right)}, \tag{12}$$

$$\Delta\xi = \frac{\varepsilon\rho_w}{(1-\varepsilon)\rho_r} - \frac{\varepsilon S_{wres}\rho_w}{(1-\varepsilon)\rho_r}, \tag{13}$$

where ε is the porosity of the rock mass; S_{wres} is the residual saturation of pore water; L_f is the latent heat per unit volume in the frozen state; k_1, k_2, and k_3 are the thermal conductivity of the rock mass in the frozen, mixed, and unfrozen zones, respectively, which can be expressed as

$$\begin{aligned} k_1 &= \varepsilon k_w S_{wres} + \varepsilon k_w(1 - S_{wres}) + (1-\varepsilon)k_w, \\ k_2 &= \varepsilon k_w S_w + \varepsilon k_i(1 - S_w) + (1-\varepsilon)k_r, \\ k_3 &= \varepsilon k_w + (1-\varepsilon)k_r, \end{aligned} \tag{14}$$

where S_w is the saturation of water; k_w, k_i, and k_r are the thermal conductivity of water, ice, and rock, respectively; c_1, c_2, and c_3 are the specific heat capacities of rock in the frozen, mixed, and unfrozen zones, respectively, which can be expressed as

$$\begin{aligned} c_1 &= \varepsilon\rho_w c_w S_{wres} + \varepsilon\rho_i c_i(1 - S_{wres}) + (1-\varepsilon)\rho_r c_r, \\ c_2 &= \varepsilon\rho_w c_w S_w + \varepsilon_w c_i(1 - S_w) + (1-\varepsilon)\rho_r c_r, \\ c_3 &= \varepsilon\rho_w C_w + (1-\varepsilon)\rho_r c_r, \end{aligned} \tag{15}$$

where c_r, c_w, and c_i are the heat capacities of rock, water, and ice, respectively; ρ_r, ρ_w, and ρ_i are the densities of rock, water, and ice, respectively.

In order to reduce the influence of surface air temperature on the tunnel lining temperature field, the thickness of the surrounding rock above the tunnel in the cold zone is greater than the standard freezing depth of the tunnel site area. Suppose the radius of influence of the buried temperature field is known, in that case, the temperature field at the outer boundary of the tunnel temperature field influence circle can be calculated with the $f_2(\bullet)$.

$$\begin{aligned} T_d(\theta,t) &= \left(T_f - T_0\right)\frac{f_2(R\sqrt{\alpha_3 t}/2)}{f_2(\gamma\sqrt{\alpha_4/\alpha_3})} + T_0, \\ R &= d_R + r_d[1 - \sin(\theta)]. \end{aligned} \tag{16}$$

After determining the temperature field at the outer boundary of the cold tunnel influence circle, the complex heat transfer problem in the shallow buried section of the cold tunnel can be transformed into a heat transfer problem in a circular multilayer medium.

The outer boundary conditions for the temperature field in the shallow section of the tunnel where the temperature at the outer boundary changes with time are calculated by the

following equation.

$$T_d(\theta, t) = \left(T_f - T_0\right)\frac{f_2(R\sqrt{\alpha_3 t}/2)}{f_2(\gamma\sqrt{\alpha_4/\alpha_3})} + T_0. \tag{17}$$

According to the structural characteristics of the tunnel and the law of temperature distribution, the temperature of the surrounding rock at the location of the vault in the tunnel cross-section ($\theta = \pi/2$) is the lowest; the temperature of the surrounding rock at the maximum freezing depth $Z_2(t) = z_0$ is the lowest temperature; in order to meet the needs of the tunnel to prevent freezing and keep warm to the maximum and to facilitate theoretical calculations, according to the principle of the most unfavorable design calculation, the temperature at $\theta = \pi/2$ and $Z_2(t) = z_0$ is taken as the temperature at the outer boundary of the influence layer of the tunnel temperature field is obtained:

$$T_0 = \frac{1}{4\alpha_4}\left(\frac{z_0}{\gamma}\right), \tag{18}$$

where z_0 is the standard freezing depth for the area.

The inner boundary of the heat transfer calculation model for the shallow buried section of the tunnel is the convective heat exchange that occurs between the air inside the cave and the cave wall. Once the internal and external boundary conditions have been determined, the formulae for solving the tunnel temperature field can be derived.

According to the assumptions, the thermal resistance of the contact between the multilayer media is neglected. The contact boundary temperature and heat flow are equal, i.e., the contact boundary between the multilayer media satisfies.

$$\begin{aligned} T_i(r_i, t) &= T_{i+1}(r_i, t), \\ k_i\frac{\partial T_i(r_i, t)}{\partial r} &= k_{i+1}\frac{\partial T_{i+1}(r_i, t)}{\partial r}. \end{aligned} \tag{19}$$

Tunnel construction inevitably affects the initial temperature field of the surrounding rock. Based on the air and surrounding rock temperature characteristics in the cavern, the initial temperature field $f(r)$ (steady-state temperature field) is determined by the annual average air temperature, the actual ground temperature of the surrounding rock.

$$T(r, 0) = f(r). \tag{20}$$

Using the superposition principle and the Laplace transform method, the theoretical solution of the radial temperature field of the tunnel lining and the surrounding rock in the cold zone is

$$T(r, t) = \mathrm{Re}\left[F(\omega, r)T_{A,i,n}(z)e^{i(at+\varphi)}\right] + \bar{F}(r).T_{M,\mathrm{in}}(z) + \bar{G}(r)T_d. \tag{21}$$

3.3. Thermal Coupling Theory. In order to facilitate the quantitative analysis of the state of deterioration, assumptions are made: (1) the unfrozen soil in the cavity behind the wall is considered to be anisotropic material; (2) the migration of heat during the change of water from liquid to solid is not considered; (3) the pressure value at which water changes to ice remains constant.

According to the first law of thermodynamics and the basic theory of heat transfer, the temperature change inside the cavity space follows the law of energy conservation and simplifying the nonstationary heat conduction equation yields

$$\frac{\partial T}{\partial t} = \alpha\left(\frac{\partial^2 T}{\partial x^2} + \frac{\partial^2 T}{\partial y^2} + \frac{\partial^2 T}{\partial z^2}\right) + \frac{q_v}{c\gamma}, \tag{22}$$

where T is the cavity space temperature; t is time; α is the thermal diffusivity of the lining; q_v is the heat released per unit volume per unit time; γ is the volumetric weight of the lining; c is the thermal diffusivity of the lining.

The heat conduction equation was discretized using the Galliakin method and the weighted residual method in the postwall cavity range Ω [6].

$$\iiint_\Omega W\left[\begin{array}{c}\left(\dfrac{\partial^2 T}{\partial x^2} + \dfrac{\partial^2 T}{\partial y^2} + \dfrac{\partial^2 T}{\partial z^2}\right) - \\ \dfrac{1}{\alpha}\left(\dfrac{q_v}{\lambda} - \dfrac{\partial T}{\partial t}\right)\end{array}\right] dxdydz = 0, \tag{23}$$

where W is the weight function; λ is the thermal conductivity of the cavity wall.

The thermodynamic coupled stress-strain control equation can be obtained for the cavity conditions behind the tunnel lining wall.

$$\begin{aligned} \frac{\partial \sigma_x}{\partial x} + \frac{\partial \tau_{yx}}{\partial y} + \frac{\partial \tau_{zr}}{\partial z} &= f_x, \\ \frac{\partial \tau_{xy}}{\partial x} + \frac{\partial \sigma_y}{\partial y} + \frac{\partial \tau_{zy}}{\partial z} &= f_y, \\ \frac{\partial \tau_{xz}}{\partial x} + \frac{\partial \tau_{yz}}{\partial y} + \frac{\partial \sigma_z}{\partial z} &= f_z, \end{aligned} \tag{24}$$

$$\varepsilon = \frac{1}{2}\left(\nabla u + (\nabla u)^T\right), \tag{25}$$

$$\sigma = \frac{E_\mu}{(1+\mu)(1-2\mu)}\left(\varepsilon_x + \varepsilon_y + \varepsilon_z\right) + \frac{E}{(1+\mu)}\varepsilon. \tag{26}$$

When $T < 0 \circ \mathrm{C}$, as Figure 4 shows.

$$\varepsilon_{wi} = \frac{1}{2}\left(\frac{\rho_w}{\rho_i} - 1\right)\theta_w. \tag{27}$$

f is the body stress; σ is a positive stress; τ is the shear stress; E is the modulus of elasticity; μ is the Poisson's ratio; ε is a positive strain; u is the displacement vector; ε_{wi} is the strain resulting from the coupling of temperature and water.

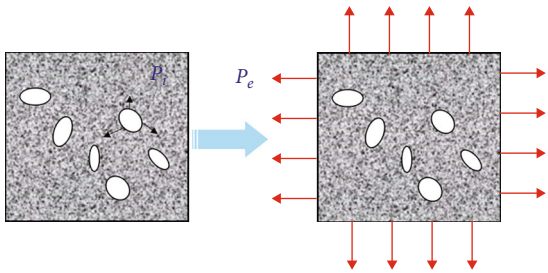

Figure 4: Frozen expansion force of the cavity.

The tunnel thermal-structural coupling problem, where the structural stress has a small effect on temperature and the temperature has a significant effect on the structural strain, is therefore analyzed using a one-way coupling method, where the temperature from the thermal analysis is applied as a thermal load to the structural analysis, as shown in the following equation.

$$u = f(T). \tag{28}$$

4. Numerical Calculation Model

4.1. Defining Shape Functions.

$$\begin{cases} T = N^T \bar{T}, \\ \begin{bmatrix} \dfrac{\partial T}{\partial x} \\ \dfrac{\partial T}{\partial y} \\ \dfrac{\partial T}{\partial z} \end{bmatrix} = B_T \bar{T}, \\ \dfrac{\partial T}{\partial t} = N \dfrac{\partial \bar{T}}{\partial t}, \end{cases} \tag{29}$$

where N^T and B_T are the vector-matrix; $\bar{T}$ is the unit node temperature.

The thermal coupling equation (30) is obtained by combining the theoretical formulation and the finite element shape function equation. The temperature values of the nodes in the central region can be obtained by using the ANSYS solver.

$$\mathrm{RT}_r + S\frac{\partial T_r}{\partial t} = P, \tag{30}$$

where T_r is the temperature column matrix.

$$\begin{cases} R = \sum_e \left(\iiint_\Omega B_t^T B_t dxdydz + \dfrac{\beta}{\lambda} \iint_S NN^T ds \right), \\ S = \sum_e \left(\iiint_\Omega \dfrac{1}{\alpha} NN^T dxdydz \right), \\ P = \sum_e \left(\iiint_\Omega \dfrac{1}{\alpha} NN^T dxdydz + \dfrac{\beta T_a}{\lambda} \iint_S N^T ds \right), \end{cases} \tag{31}$$

where β is the exothermic coefficient of the media surface; T_a is the external temperature; s is the contact area of the lining and the cavity behind the wall; e is the collection of the cavity behind the wall and the lining.

Volume changes due to temperature stresses mainly cause frost damage of tunnel linings in cavity spaces. Based on the strain increment method and the temperature values of the nodes mentioned above, the equivalent nodal loads due to creep and volume expansion are calculated according to the following equation.

$$\Delta\{R\} = \int [B]^T [D](\Delta\{\varepsilon^c\} \pm \Delta\{\varepsilon^v\}) dv, \tag{32}$$

where $\Delta\{\varepsilon^c\}$ is the creep strain increment matrix; $\Delta\{\varepsilon^e\}$ is the expansion deformation increment matrix; v is the postwall cavity range; $[B]$ is the unit shape function; $[D]$ is the lining temperature-dependent plasticity matrix; $\Delta\{R\}$ is taken as positive for icing and harmful for melting.

4.2. Delimitation Conditions

4.2.1. Initial Conditions.

$$T_i|_{t=0} = T_0(x, y, z), \tag{33}$$

where $T_i\,(i = r, w)$ is the initial conditions for the lining temperature field and the initial conditions for the temperature field in the cavity behind the wall, respectively; T_0 is the boundary temperature.

4.2.2. Boundary Conditions.

$$-\lambda_i \frac{\partial T_i}{\partial n}\bigg|_{s(x,y,z,t)} = \beta(T_r - T_w), \tag{34}$$

where n is normal; $s(x, y, z, t)$ is the surface area of the contact surface; $\lambda_i\,(i = r, w)$ denotes the thermal conductivity of the lining and the thermal conductivity of the medium in the cavity behind the wall, respectively.

4.2.3. Boundary Coupling Conditions. The intersection of the lining and the cavity behind the wall is the coupling surface, subject to two conditions.

$$\begin{cases} T_w = T_r, \\ \lambda_r \dfrac{\partial T_r}{\partial n} = \lambda_w \dfrac{\partial T_w}{\partial n}. \end{cases} \tag{35}$$

4.3. Computational Models. The numerical model is based on the main cavern of the DLJ tunnel. In order to highlight the effect of localized behind-wall voids on the deterioration of the secondary lining, the numerical simulations in this paper do not consider the effect of tunnel burial depth on the cracking of the tunnel lining structure but mainly consider the failure of the lining bearing capacity due to lining concrete crushing, tension cracking, and crack extension. The maximum principal stress failure criterion is used for the extension of lining cracks. The DLJ tunnel has a

Figure 5: The DLJ tunnel lining cracking and water seepage flooding.

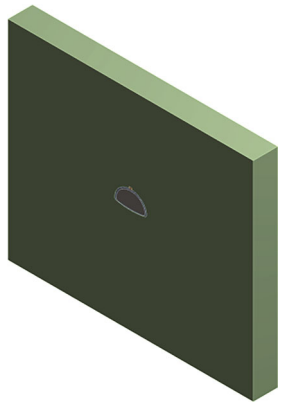

Figure 6: Computational model.

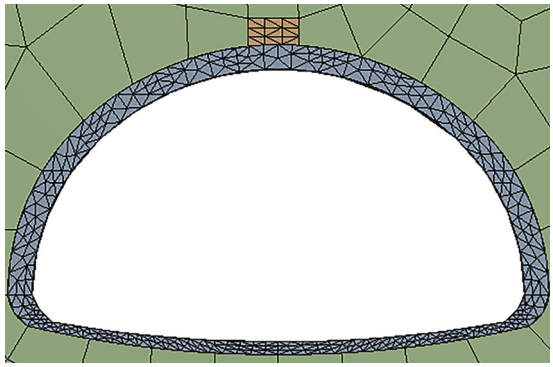

Figure 7: Partial grid refinement.

composite lining with a thickness of 60 cm. The inner profile of the tunnel is a curved-wall, equal-section, three-center circle with a vault height of 7.0 m. The net width is 10.5 m. Long-term monitoring data and data from the DLJ tunnel maintenance and improvement works in 2018 show that the tunnel has 23 circumferential cracks in the lining, including approximately four circumferential through cracks, with a width of 0.5 m. 4 cracks with a width of 0.1 ~ 5.0 mm and a length of 10~130 mm. most of the circumferential cracks have the phenomenon of water seepage and alkali flooding The width of these cracks ranges from 0.2 to 0.6 mm, and the length of these cracks ranges from 5.0 to 16.0 m. Most of the diagonal cracks have the phenomenon of water seepage and alkali flooding; there are two cross cracks in the lining. They are mainly concentrated in the top of the vault and the sidewall, with the crack width ranging from 0.2 to 0.5 mm, and most of the cross cracks have the phenomenon of water seepage and alkali flooding (as shown in Figure 5). Based on the above-cracked condition of the DLJ tunnel lining, one of the monitoring sections was selected, and the location and size of the water body in this section were identified by geo-radar and input hydrostatic level meter.

According to the characteristics of the Dulongjiang tunnel, which shows cracking of the vault lining, complex geological conditions, and significant differences in the temperature environment inside and outside the tunnel, and considering the situation of water-bearing cavities behind the tunnel lining, the MADPL module of ANSYS was used to realize the numerical simulation analysis of the cold zone tunnel thermal coupling. The calculation model is shown in Figure 6.

As the distance from the center of the tunnel increases, the temperature of the tunnel envelope is gradually reduced by the influence of the air in the tunnel, so the model was chosen to calculate a height of 100 m and a width of 100 m. The model includes the envelope, lining, water, and air, assuming that the air is an ideal gas, not compressible, and the pressure does not change with temperature. The lining in the model has a certain thickness. The cavity size behind the lining is $0.5 \times 0.65 \times 1.0$ m. To ensure the accuracy of the calculation, the lining and the cavity behind the lining are locally meshed and refined as shown in Figure 7. In order to ensure the accuracy of the calculation, the lining and the cavity behind the lining are partially refined as shown in the figure, considering that there are 68220 cells in the lining cavity calculation model.

According to the engineering design data a, the thermodynamic parameters of the calculated model can be obtained as shown in Table 1. The vertical displacement is constrained at the bottom of the model, the standard displacement is constrained at the front and back of the model, the horizontal displacement is constrained at both sides of the model, and the upper surface of the model is a free boundary with fixed constraints. Without considering the heat transfer effect of the air, the heat transfer between the liner and the air is convective, with a convective heat transfer coefficient of $a = 15$ (W/m^2•°C). According to the tunnel design data,

Table 1: Calculation of thermodynamic parameters of model materials.

Materials	Specific heat capacity J/kg•°C	Thermal conductivity W/m•°C	Coefficient of thermal expansion °C^{-1}	Density kg/m^3	Elastic modulus MPa	Poisson's ratio	Cohesion MPa	Internal friction angle°
Surrounding rocks	698	2.26	0.6×10^{-5}	2000	1500	0.4	0.22	34
Lining	960	3.01	0	2800	32000	0.2		
Air	1	—	—	1.29	—	—		
Water	4 200	0.6	5.1×10^{-5}	1000	2160	0.49		

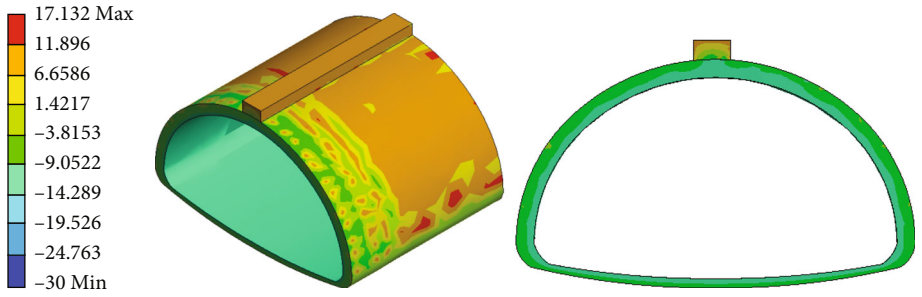

Figure 8: Temperature cloud of lining structure at air temperature -10°C.

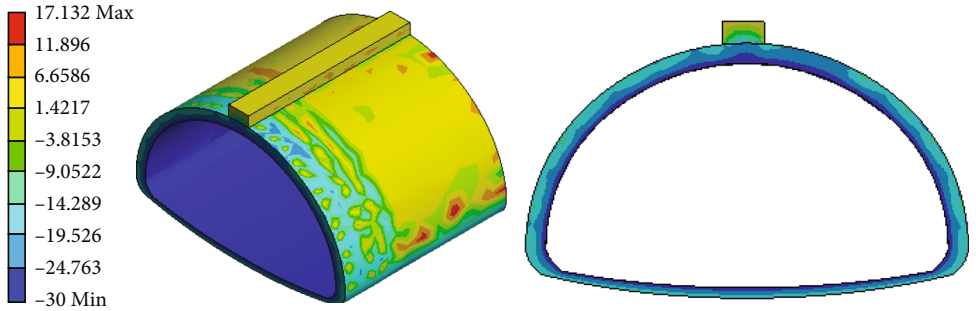

Figure 9: Temperature cloud of lining structure at air temperature -30°C.

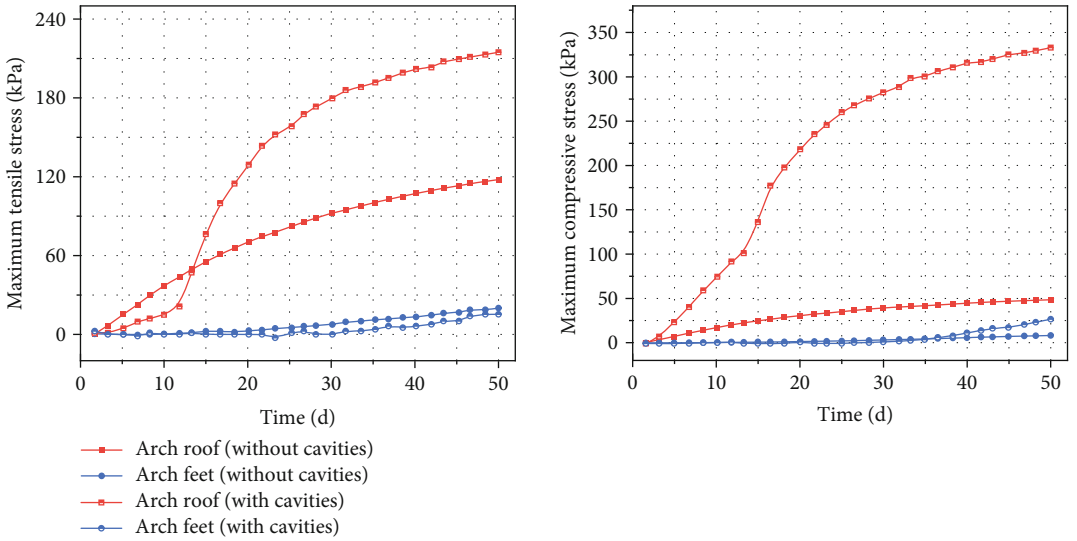

Figure 10: Internal structural forces at -10°C air temperature under w/ and w/o water-bearing cavities.

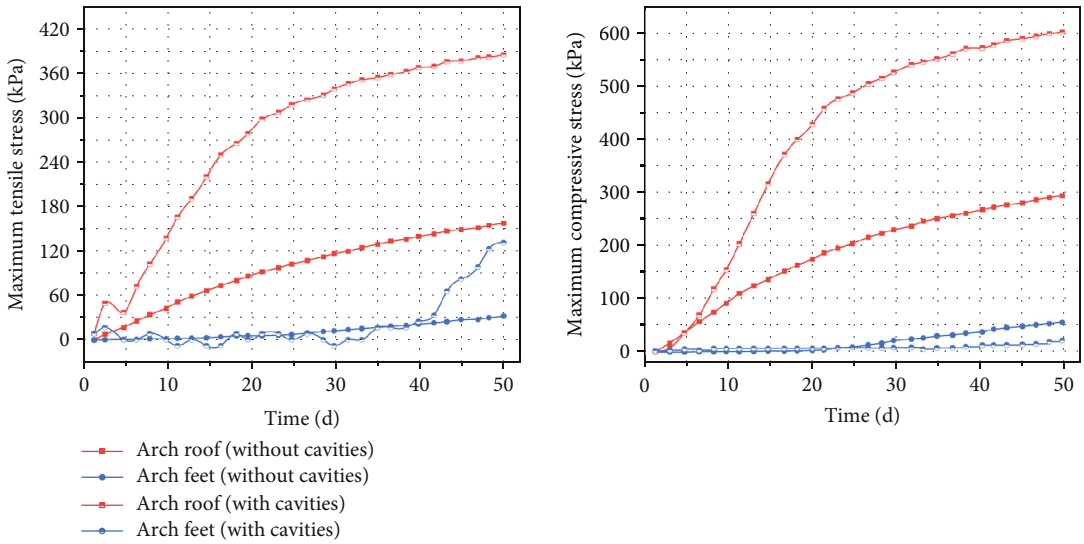

Figure 11: Internal structural forces at -30°C air temperature under w/ and w/o water-bearing cavities.

Table 2: Internal structural forces without water-bearing cavities.

Ambient temp, °C	Top of the vault		Foot of the vault	
	Max. tensile stress, kPa	Max. compressive stress, kPa	Max. tensile stress, kPa	Max. compressive stress, kPa
-10	119.6	48.2	20.1	8.2
-30	169.8	295.8	31.2	51.5
% increase	42%	514%	55%	528%

the average ground temperature in the area is 0.5°C. Then, the initial temperature of the surrounding rock can be obtained by increasing the geothermal gradient in the permafrost by 2.5%, calculating the geothermal heat flow density at the base of the model $q = 0.06\ \mathrm{W/m^2}$. The heat of the phase change of the surrounding rock of 8.21 kJ/kg is considered in the calculation process. The thermal conductivity of the surrounding rock is taken to be 2.26 W/(m.°C) by thermal conductivity determination. In order to verify the influence of air temperature on the tunnel structure, two working conditions were chosen: -10°C and -30°C. The calculations were carried out for 50 days.

5. Analysis of Calculation Results

5.1. Air Temperature Sensitivity Analysis of the Lining Structure. In order to facilitate the convergence of the model, the water storage space is assumed to be a semiellipsoid, and the process of numerical simulation does not take into account the effect of temperature changes on the stresses in the lining structure but only calculates the additional stresses generated by the local water storage space and the effect of freeze-thaw cycles on the deterioration of the secondary lining.

In order to study the sensitivity of the lining structure to temperature, the internal forces and displacements of the lining structure were calculated for the air temperature of -10°C and -30°C, respectively. The temperature calculation clouds of the lining structure under the two working conditions are as shown in Figures 8 and 9. The temperature calculation clouds for the lining structure under the two working conditions are shown in the figure below.

From the temperature calculation cloud chart, it can be seen that when the air temperature is -30°C, its temperature distribution is uneven compared to -10°C. At the location near the vault, the heat transfer in the vault part is not sufficient compared to other parts due to the water-containing cavity behind the lining, and it is low in the vault part. At -10°C, the average temperature at the top of the lining vault was -8.22°C and at the foot of the vault -6.58°C. At -30°C, the average temperature at the top of the lining vault was -26.65°C, and at the foot of the vault -19.41°C. Due to the existence of water-laden cavities behind the tunnel lining, the tunnel lining structure exhibits different temperature sensitivity under the effect of different temperatures. The lower the temperature, the more uneven the temperature distribution of the lining structure. The internal forces of the structure without/with a water-bearing cavity behind the lining are calculated as shown in Figures 10 and 11.

Analyzing the effect of temperature on the lining structure, it can be seen that the lower the temperature, the more pronounced the effect on the lining structure, and regardless of whether there is a water-bearing cavity behind the lining, as the calculation time increases, the internal force of the lining structure increases, indicating that the more thoroughly the tunnel lining structure and air heat exchange is affected by the air temperature, at the 50th day of calculation, the internal force of the lining structure gradually tends to stabilize.

When the ambient temperature is -10°C, the internal forces in the lining structure are mainly tensile stresses, with a maximum tensile stress of 119.6 kPa and maximum compressive stress of 48.2 kPa at the top of the vault and maximum tensile stress of 20.1 kPa and maximum compressive

Table 3: Internal structural forces with water-bearing cavities.

Ambient temp, ˚C	Top of the vault		Foot of the vault	
	Max. tensile stress, kPa	Max. compressive stress, kPa	Max. tensile stress, kPa	Max. compressive stress, kPa
-10	212.8	362.4	15.3	26.2
-30	382.6	598.8	126.5	31.8
% increase	80%	65%	727%	21%

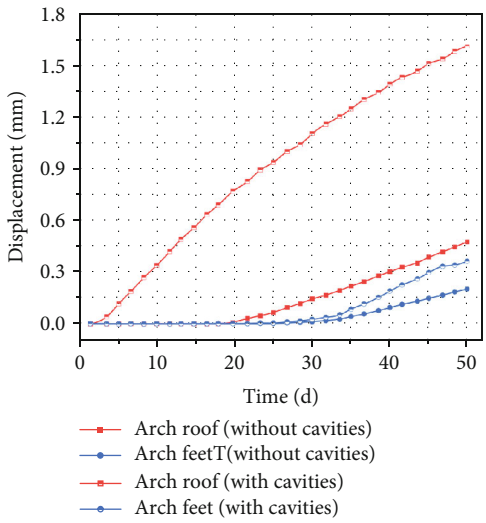

Figure 12: Lining displacement without water-bearing cavities.

stress of 8.2 kPa at the foot of the vault. When the ambient temperature is -30˚C, the internal forces in the lining structure are mainly compressive stresses, with a maximum tensile stress of 169.8 kPa at the top of the vault and maximum compressive stress of 295.8 kPa, an increase of 513.63% compared to the ambient temperature of -10˚C. The maximum tensile stress at the top of the arch is 169.8 kPa, an increase of 41.98% compared to the ambient temperature of -10˚C. The maximum compressive stress is 295.8 kPa, an increase of 513.63%; the maximum tensile stress at the foot of the arch is 31.2 kPa, an increase of 55.22%; and the maximum compressive stress is 51.5 kPa, an increase of 528.05%. Thus, as the ambient temperature decreases, the internal force of the lining structure is changed from mainly tensile stress to mainly compressive stress. The compressive stress affects different locations of the lining structure to different degrees. The compressive stress at the top of the vault is more significant than that at the foot of the vault, with a stress ratio of 474.36%, and an obvious stress concentration phenomenon at the top of the vault. The specific research results are shown in Table 2.

In the case of a water-bearing cavity behind the tunnel lining, the internal force curve increases abruptly at 12 d for the -10˚C ambient temperature condition, which is analyzed as the water in the cavity starts to freeze. In contrast, for the -30˚C ambient temperature condition, the internal force curve changes smoothly, indicating that the water in the cavity freezes in 1-2 d due to the shallow ambient temperature. The ambient temperature of -10˚C and -30˚C both show that compressive stresses dominate the internal force at the vault of the lining structure, but the difference between tensile and compressive stresses is relatively tiny. When the ambient temperature is -10˚C, the maximum tensile stress at the top of the arch is 212.8 kPa, and the maximum compressive stress is 362.4 kPa; the maximum tensile stress at the foot of the arch is 15.3 kPa, and the maximum compressive stress is 26.2 kPa. When the ambient temperature is -30˚C, the maximum tensile stress at the top of the arch is 382.6 kPa, increasing the stress ratio by 79.79%; and the maximum compressive stress is 598.8 kPa, increasing the stress ratio by 65.23%. The maximum tensile stress at the foot of the arch is 126.5 kPa, with an increased stress ratio of 726.69%, and the maximum compressive stress is 31.8 kPa, with an increased stress ratio of 21.36%. Thus, in the case of a cavity behind the lining, the internal forces of the lining structure show uneven characteristics. The stresses at the top of the arch are concentrated, and as the ambient temperature decreases, the stresses at the top of the arch are concentrated. The internal forces at the foot of the arch are converted from mainly compressive stresses to mainly tensile stresses. The specific research results are shown in Table 3.

5.2. Impact of Water-Laden Voids on Lining Structures. In order to investigate the effect of water voids behind the lining on the lining structure, the internal forces and displacements of the lining structure were calculated for the absence and presence of water voids behind the lining. At an ambient temperature of -30˚C, the lining structure's displacements at different locations are shown in Figure 12.

As can be seen from the above figure, when the ambient temperature is -30˚C, the frost expansion of the water-bearing cavity behind the lining has a weak effect on the displacement at the foot of the arch. The maximum displacement at the foot of the arch changes from 0.2 mm to 0.24 mm, and its increase is mainly due to the increased deformation at the top of the arch, i.e., the deformation of the water-bearing cavity behind the lining at the foot of the arch is indirect. The maximum deformation at the top of the arch increased from 0.48 mm to 1.61 mm, an increase of 235.42%, which is due to the frost expansion of the water-bearing cavity acting as a significant downward force on the top of the arch, causing the deformation at the top of the arch to increase. In addition, when there is no water-bearing cavity behind the lining, the deformation time of the vault top and footing is around 20 d, while when there is a water-bearing cavity behind the lining, the deformation time of the vault top is earlier, and the deformation time of the footing is delayed.

It can be seen that the presence of a water-bearing cavity behind the tunnel lining has a significant effect on the internal forces of the lining structure compared to the absence of a water-bearing cavity, with both ambient temperature conditions showing a significant increase in internal forces in the lining structure. Taking the ambient temperature of -30 degrees Celsius as an example, the maximum tensile stress

at the top of the arch is 169.8 kPa, and the maximum compressive stress is 295.8 kPa, while the maximum tensile stress at the foot of the arch is 31.2 kPa, and the maximum compressive stress is 51.5 kPa in the case of a water-bearing cavity behind the lining. 125.32%, maximum compressive stress 598.8 kPa, 102.43%, maximum tensile stress 126.5 kPa, 305.45%, maximum compressive stress 31.8 kPa, -38.24% at the foot of the arch. Due to the existence of the water-bearing cavity behind the lining, the frost swelling force at the top of the arch increases, and the tensile stress at the foot of the arch also increases significantly. The results obtained in this paper agree with the previous study [2–5] on the stress and deformation laws of tunnels in five cold regions of China.

6. Conclusion

The temperature difference between the ambient temperature and the internal temperature of the surrounding rocks in tunnels in the freezing season is so great that the tunnel lining structure often faces the problem of frost heave damage, especially when the existing tunnel lining structure has broken rings. To study the effect of freezing and to swell on the lining structure, this paper uses a combination of field tests and ANSYS numerical simulations to establish a coupled thermal model of the lining structure, taking into account the temperature effect and analyzing the effect of ambient temperature and the cavity behind the lining on the internal force and deformation of the lining structure. The results show that the ambient temperature and the cavity behind the lining significantly impact the structure's safety. The internal force of the tunnel lining structure increases as the ambient temperature decreases, and stress concentration occurs at the top of the vault. Water-laden voids increase deformation at the top of the vault and an earlier deformation time, while the deformation time at the foot of the vault is delayed. In this paper, the effect of the presence or absence of water voids on the internal forces of the lining structure at ambient temperatures of -10°C and -30°C is compared and investigated by establishing a calculation model that takes into account the effect of water voids and temperature behind the tunnel lining, and the following conclusions are drawn.

(1) In the absence of a water-bearing cavity behind the tunnel lining, the internal forces in the tunnel lining structure increase as the ambient temperature decreases, and the internal forces in the structure are converted from tensile stress dominant to compressive stress dominant, with a maximum tensile stress increase stress ratio of 41.98% and a maximum compressive stress increase stress ratio of 513.63% at the top of the vault

(2) The tunnel lining structure is not uniformly stressed by the freezing force, and the stress is concentrated at the top of the vault. Under the condition of water-free cavity, the compressive stress at the top of the vault is 474.36% higher than the stress at the foot of the vault when the ambient temperature is -10°C

(3) In the case of a water-bearing cavity behind the tunnel lining, the stress at the top of the vault is significantly increased due to the effect of the freezing and expansion of the water-bearing cavity, with a maximum tensile stress of 382.6 kPa and maximum compressive stress of 598.8 kPa. In contrast, the stress at the foot of the vault varies unevenly, with the tensile stress increasing and the compressive stress decreasing

(4) The existence of water-bearing cavities leads to an increase in deformation at the vault position, with the maximum deformation at the vault position increasing from 0.48 mm to 1.61 mm, an increase of 235.42%, and the deformation time at the vault position is advanced. In contrast, the deformation time at the foot position is delayed

(5) The ambient temperature and the water cavity behind the lining have a more significant impact on the safety of the lining structure. From the perspective of structural safety, it is recommended that thermal insulation measures and slurry sealing of the cavity behind the lining be adopted

(6) The double superposition effect of extreme ambient temperature and water-bearing cavity behind the lining greatly influences the safety of the lining structure. According to previous construction experience [29–36], appropriate engineering measures for the two factors are taken, respectively. Laying polyphenolic insulation board on the lining surface and grouting filling method to seal the cavity behind the lining have proven effective measures

In this paper, the tunnel heat transfer model is assumed to be a multilayer radial heat transfer model, which is equivalent to the multilayer plate constant heat flow heat transfer model, and the contact thermal resistance and axial heat transfer are ignored. In the case of thermal stress failure, the team will further study the superposition failure mechanism of thermal stress in the loss mode of the lining structure and the influence range of water-bearing cavity location on temperature stress concentration of lining structure.

Data Availability

The experimental data used to support the findings of this study are included within the article.

Conflicts of Interest

The authors declare that they have no known competing financial interests or personal relationships that could have appeared to influence the work reported in this paper.

References

[1] Y. M. Lai, S. Y. Liu, Z. W. Wu, and W. B. Yu, "Approximate analytical solution for temperature fields in cold regions circular tunnels," *Cold Regions Science and Technology*, vol. 34, no. 1, pp. 43–49, 2002.

[2] Y. L. Yuan and Y. M. Lai, "The identification and classification of freezing-thawing and frozen environments for the surrounding rocks of tunnels in cold regions," *Modern Tunnelling Technology*, vol. 53, no. 3, pp. 19–25, 2016, (in Chinese).

[3] S. Y. Li, F. R. Niu, Z. Z. Sun, and H. S. Shi, "Numerical study on moisture-heat-mechanics coupled process of Jiangluling tunnel construction in permafrost region," *Journal of Glaciology and Geocryology*, vol. 40, no. 5, pp. 966–973, 2018, (in Chinese).

[4] Y. A. O. Hong-zhi, Z. H. A. N. G. Xiao-xu, D. O. N. G. Chang-song, and F. A. N. Dong-fang, "Comparison analysis on heat insulating material property laying way of highway tunnel in permafrost regions," *China Journal of Highway and Transport*, vol. 28, no. 12, pp. 106–113, 2015, (in Chinese).

[5] Y. Zeng, K. Liu, X. Zhou, and L. Fan, "Tunnel temperature fields analysis under the couple effect of convection- conduction in cold regions," *Applied Thermal Engineering*, vol. 120, pp. 378–392, 2017.

[6] N. Barton, "Shear strength criteria for rock, rock joints, rockfill and rock masses: problems and some solutions," *Journal of Rock Mechanics and Geotechnical Engineering*, vol. 5, no. 4, pp. 249–261, 2013.

[7] M. Bahaaddini, P. C. Hagan, R. Mitra, and B. K. Hebblewhite, "Scale effect on the shear behaviour of rock joints based on a numerical study," *Engineering Geology*, vol. 181, pp. 212–223, 2014.

[8] S. Du, Y. Hu, and X. Hu, "Measurement of joint roughness coefficient by using profilograph and roughness ruler," *Journal of Earth Science*, vol. 20, no. 5, pp. 890–896, 2009.

[9] G. Z. Zhang, C. C. Xia, and X. G. Ma, "Rock-soil thermal response test of tunnel heating system using heat pump in cold region," *Chinese Journal of Rock Mechanics and Engineering*, vol. 31, no. 1, pp. 99–105, 2012, (in Chinese).

[10] Q. Feng and B. S. Jang, "Analytical method for insulation layer thickness of highway tunnels with multilayer dielectric in cold regions," *Chinese Journal of Geotechnical Engineering*, vol. 36, no. 10, pp. 1879–1887, 2014, (in Chinese).

[11] N. I. E. Feng-ming, "The air temperature condition of railway tunnel in cold area," *Journal of Glaciology and Geocryology*, vol. 10, no. 4, pp. 450–453, 1988, (in Chinese).

[12] S. Li, K. G. Sun, W. G. Qiu, W. P. Xu, and L. P. Li, "Influence and sensitivity analysis of surrounding rock thermal parameters on temperature field of cold region tunnel," *China Civil Engineering Journal*, vol. 50, pp. 117–122, 2017, (in Chinese).

[13] T. Yamabe and K. M. Neaupane, "Determination of some thermo-mechanical properties of Sirahama sandstone under subzero temperature condition," *International Journal of Rock Mechanics and Mining Sciences*, vol. 38, no. 7, pp. 1029–1034, 2001.

[14] Z. Zhang, S. H. Wang, T. J. Yang, and Y. N. Zhang, "Numerical analysis on hydro thermal coupling of surrounding rocks in cold region tunnels," *Journal of Northeastern University (Natural Science)*, vol. 41, no. 5, pp. 635–641, 2020, (in Chinese).

[15] J. L. Qi and W. Ma, "Mechanical properties and research status of frozen soil," *Rock and Soil Mechanics*, vol. 31, no. 1, pp. 133–143, 2010, (in Chinese).

[16] T. Xian-jun, Y. Xiang-hong, and C. Wei-zhong, "Temperature field research and engineering application of geotechnical media during freezing and thawing process," *Chinese Journal of Geotechnical Engineering*, vol. 31, no. S1, pp. 2867–2874, 2012, (in Chinese).

[17] Y. M. Lai, Z. W. Wu, Y. L. Zhu, and L. Zhu, "Nonlinear analysis for the coupled problem of temperature and seepage fields in cold regions tunnels," *Cold Regions Science and Technology*, vol. 29, no. 1, pp. 89–96, 1999.

[18] Y. M. Lai, Z. W. Wu, Y. L. Zhu, and L. N. Zhu, "Nonlinear analysis for the coupled problem of temperature, seepage and stress fields in cold-region tunnels," *Tunnelling and Underground Space Technology*, vol. 13, no. 4, pp. 435–440, 1998.

[19] Y. M. Lai, Z. W. Wu, and Y. L. Zhu, "Analytical viscoelastic solution for frost force of cold regional tunnels," *Journal of the China Railway Society*, vol. 21, no. 6, pp. 70–74, 1999, (in Chinese).

[20] X. F. Zhang, Y. M. Lai, W. B. Yu, and Y. P. Wu, "Forecast and analysis of refreezing in Fenghuoshan permafrost tunnel," *Chinese Journal of Rock Mechanics and Engineering*, vol. 23, no. 24, pp. 4170–4178, 2004, (in Chinese).

[21] Z. Xuefu, L. Yuanming, Y. Wenbing, and Z. Shujuan, "Nonlinear analysis of three-dimensional temperature field in cold zone tunnels," *Journal of Civil Engineering*, vol. 7, no. 2, pp. 47–53, 2004, (in Chinese).

[22] H. Q. Xie, C. He, and Y. L. Li, "Study on the phase change temperature field of insulation thickness in highway tunnels in cold areas," *Journal of Rock Forces and Engineering*, vol. 26, no. S2, pp. 4395–4401, 2007, (in Chinese).

[23] B. Yuan, M. Sun, L. Xiong, Q. Luo, S. Pradhan, and H. Li, "Investigation of 3D deformation of transparent soil around a laterally loaded pile based on a hydraulic gradient model test," *Journal of Building Engineering.*, vol. 28, no. 3, p. 101024, 2020.

[24] J. F. Huang, C. C. Xia, C. L. Han, and Z. Li, "Distribution and simplified calculation method of the frost heaving force of highway tunnels in cold regions," *Modern Tunnel Technology*, vol. 53, no. 5, pp. 63–70, 2016, (in Chinese).

[25] B. Yuan, Z. Li, Z. Zhao, H. Ni, Z. Su, and Z. Li, "Experimental study of displacement field of layered soils surrounding laterally loaded pile based on transparent soil," *Journal of Soils and Sediments*, vol. 21, no. 9, pp. 3072–3083, 2021.

[26] Y. W. Wang and J. Y. Zheng, "Study of simplified mechanical models of frost-heaving of water behind highway tunnel lining and its error analysis," *Tunnel Construction*, vol. 38, no. S1, pp. 104–109, 2018, (in Chinese).

[27] Y. S. Li and S. G. Chen, "Analytical solution of frost heaving force in nor-circular cold region tunnels," *Chinese Journal of Theoretical and Applied Mechanics*, vol. 52, no. 1, pp. 196–207, 2020, (in Chinese).

[28] Y. Gao, Y. Q. Zhu, B. G. He, J. Geng, and P. Cui, "Development and application of test system modeling temperature field for high speed railway tunnel in cold region," *Chinese Journal of Rock Mechanics and Engineering*, vol. 36, no. 8, pp. 1989–1998, 2017, (in Chinese).

[29] B. Yuan, Z. Li, Y. Chen et al., "Mechanical and microstructural properties of recycling granite residual soil reinforced with glass fiber and liquid-modified polyvinyl alcohol polymer," *Chemosphere*, vol. 268, article 131652, 2022.

[30] Y. Bingxiang, S. Meng, W. Yixian, Z. Lihua, L. Qingzi, and Z. Xuqun, "Full 3D displacement measuring system for 3D

displacement field of soil around a laterally loaded pile in transparent soil," *ASCE International Journal of Geomechanics*, vol. 19, no. 5, p. 04019028, 2019.

[31] L. Wang, F. Guo, H. Yang, Y. Wang, and S. Tang, "Comparison of fly ash, PVA fiber, MgO and shrinkage-reducing admixture on the frost resistance of face slab concrete via pore structural and fractal analysis," *Fractals*, vol. 29, no. 2, p. 2140002, 2021.

[32] L. Wang, X. Lu, L. Liu et al., "Influence of MgO on the hydration and shrinkage behavior of low heat Portland cement-based materials via pore structural and fractal analysis," *Fractal and Fractional*, vol. 6, no. 1, p. 40, 2022.

[33] L. Wang, R. Y. Luo, and W. Zhang, "Effects of fineness and content of phosphorus slag on cement hydration, permeability, pore structure and fractal dimension of concrete," *Fractals*, vol. 29, no. 2, p. 2140004, 2021.

[34] C. Liu, L. Du, X. Zhang, Y. Wang, X. Hu, and Y. Han, "A new rock brittleness evaluation method based on the complete stress-strain curve," *Lithosphere*, vol. 2021, no. Special 4, article 4029886, 2021.

[35] B. Yuan, Z. Li, W. Chen et al., "Influence of groundwater depth on pile–soil mechanical properties and fractal characteristics under cyclic loading," *Fractal Fract.*, vol. 6, p. 198, 2022.

[36] C. Liu, Y. Wang, X. Hu, Y. Han, X. Zhang, and L. Du, "Application of GA-BP neural network optimized by Grey Verhulst model around settlement prediction of foundation pit," *Geofluids*, vol. 2021, Article ID 5595277, 16 pages, 2021.